Nano Energy 50 (2018) 766–776

Contents lists available at ScienceDirect

Nano Energy

journal homepage: www.elsevier.com/locate/nanoen

Full paper

Fabrication and excellent performances of $Bi_{0.5}Sb_{1.5}Te_3$/epoxy flexible thermoelectric cooling devices

Weikang Hou[1], Xiaolei Nie[1], Wenyu Zhao*, Hongyu Zhou, Xin Mu, Wanting Zhu, Qingjie Zhang*

State Key Laboratory of Advanced Technology for Materials Synthesis and Processing, Wuhan University of Technology, Wuhan 430070, China

ARTICLE INFO

Keywords:
Flexible thermoelectric device
$Bi_{0.5}Sb_{1.5}Te_3$/epoxy thick film
Hot-pressing curing
Electrical transport properties
Cooling performance

ABSTRACT

How to fabricate flexible thermoelectric (TE) films with excellent electrical transport properties remains a major bottleneck for high-performance flexible TE cooling devices. Herein, a simple and efficient method is developed to fabricate high-performance flexible TE cooling device by selecting $Bi_{0.5}Sb_{1.5}Te_3$ as TE component and epoxy resin as adhesive. It is discovered that the (000*l*) preferential orientation of $Bi_{0.5}Sb_{1.5}Te_3$ grains could be successfully realized in $Bi_{0.5}Sb_{1.5}Te_3$/epoxy thick films by hot-pressing curing process, thus causing the remarkable enhancement in the electrical transport properties. The highest power factor of the (000*l*)-oriented $Bi_{0.5}Sb_{1.5}Te_3$/epoxy thick films reached 0.84 mW m^{-1} K^{-2} at 300 K, increased by 250% and 223% as compared with that of our non-pressure thick film and the highest value by other groups, respectively. A prototype flexible TE cooling device had been fabricated with the $Bi_{0.5}Sb_{1.5}Te_3$/epoxy thick films. The stable temperature difference of the prototype device reached 6.2 K under a working current of 0.06 A, increased by about 24% as compared with the highest temperature difference of 5 K reported by other groups. Our work demonstrates that the hot-pressing curing process provides an effective approach to fabricate high-performance flexible TE cooling devices with $Bi_{0.5}Sb_{1.5}Te_3$/epoxy thick films through the (000*l*) preferential orientation.

1. Introduction

How to take away the harmful waste heat occurring at nonplanar local areas have posed great challenges in various microelectronic integrated devices as widely used in powerful processors or end-user operation platforms [1–4]. The thermal management technology based on Peltier effect of thermoelectric (TE) materials has attracted increasing attention due to a series of unique advantages such as high reliability, no moving parts, good compactness, and lightweight [5–7]. However, all the currently commercial TE devices are composed of sintered bulk TE legs connected electrically in series through metallic electrodes and then sandwiched between ceramic plates [8,9]. The conventional structure has poor flexibility and thus it is very difficult to realize dimensionally good match between the commercial TE device and the electronic component. The miniaturized flexible TE devices based on TE films are highly promising to solve the bottleneck [3,4,7,10]. However, the preparation of thin films with less than 100 nm in thickness is not only time-consuming but also very inefficient. Alternatively, the thick films prepared by cost-effective printing technologies become a potential candidate for realizing miniaturization and flexibility of TE devices.

The conversion efficiency of a TE cooling device is expressed by the coefficient of performance (*COP*) [11]

$$\mathrm{COP} = \frac{T_c}{T_h - T_c} \cdot \frac{\sqrt{1+ZT} - T_h/T_c}{\sqrt{1+ZT}+1}$$

where T_h and T_c are the temperatures of the hot side and cold one of the TE device, ZT is the dimensionless figure-of-merit of TE materials $ZT = \alpha^2\sigma T/\kappa$, where T, α, σ and κ are absolute temperature, Seebeck coefficient, electrical conductivity and thermal conductivity, respectively. Apparently, a TE device with high *COP* requires high ZT of TE materials.

Great progress has been made in developing high-performance bulk TE materials in the recent two decades and several TE materials have ZT values exceeding 2.0 [12–17]. Unfortunately, when printing the high-performance bulk TE materials on the flexible substrates and transforming into flexible TE thick films with the same chemical compositions, the ZT values were greatly decreased due to the largely deteriorated electrical transport properties originating from low density and various structural defects [18,19]. Several strategies such as cold isostatic pressing, [20,21] selecting additives as sintering aids [22,23] and burning off the insulating binders via high temperature sintering [24]

* Corresponding authors.
E-mail addresses: wyzhao@whut.edu.cn (W. Zhao), zhangqj@whut.edu.cn (Q. Zhang).
[1] These authors contributed equally to this work.

https://doi.org/10.1016/j.nanoen.2018.06.020
Received 29 March 2018; Received in revised form 7 June 2018; Accepted 7 June 2018
Available online 17 June 2018

were employed to enhance the electrical transport properties of flexible TE composite thick films. However, so far, the poor electrical transport properties of flexible TE thick films are still a major bottleneck in developing high-performance flexible TE devices.

In this work, a series of $Bi_{0.5}Sb_{1.5}Te_3$/epoxy flexible thick films with (000*l*) preferential orientation were prepared on polyimide substrates by the combination of brush-printing and hot-pressing curing processes. The (000*l*)-oriented $Bi_{0.5}Sb_{1.5}Te_3$/epoxy flexible thick films exhibited excellent electrical transport properties due to the (000*l*) preferential orientation of $Bi_{0.5}Sb_{1.5}Te_3$ grains induced by the hot-pressing curing process. The highest power factor reached 0.84 mW m^{-1} K^{-2} at 300 K for $Bi_{0.5}Sb_{1.5}Te_3$/epoxy thick film cured under 623 K and 4 MPa, increased by 180% and 223% as compared with that of our non-pressure thick film and the highest value reported by other groups, respectively. The FTIR spectra show that the main structure of three-dimensional cross-linked network of epoxy resin should keep well in all the thick films cured in the temperature range of 473–623 K. A prototype flexible TE cooling device was designed and fabricated with the $Bi_{0.5}Sb_{1.5}Te_3$/epoxy thick films. The cooling performance of the prototype flexible TE device was evaluated by measuring the temperature difference between the hot side and cold one of TE legs. This work demonstrates that the hot-pressing curing process provides an effective approach to fabricate high-performance $Bi_{0.5}Sb_{1.5}Te_3$/epoxy flexible TE devices through producing the (000*l*) preferential orientation of $Bi_{0.5}Sb_{1.5}Te_3$ grains in $Bi_{0.5}Sb_{1.5}Te_3$/epoxy thick films.

2. Experimental section

2.1. Preparation of printable slurries

The slurries were made of $Bi_{0.5}Sb_{1.5}Te_3$ powder, epoxy resin, hardener, catalyst and reactive diluent [19]. Diglycidyl ether of bisphenol-F (NanYa electronic material Inc) was used as epoxy resin. Methylhexahydrophthalic anhydride (Sinopharm chemical reagent) was used as hardener. 2-ethyl-4-methylimidazole (Sinopharm chemical reagent) was used as catalyst. Butyl glycidyl ether (Sinopharm chemical reagent) was used as reactive diluent. Firstly, $Bi_{0.5}Sb_{1.5}Te_3$ ingots were crushed and pulverized with a planetary ball mill apparatus at a speed of 200 rpm for 2 h under the protection of argon. Fig. 1 shows the FESEM image of ball-milled $Bi_{0.5}Sb_{1.5}Te_3$ powders. It can be seen that the ball-milled $Bi_{0.5}Sb_{1.5}Te_3$ grains have flake-like shape, which must be re-arranged along the (000*l*) orientation or the *ab*-plane during the hot-pressure curing process based on the minimal energy principle. Secondly, epoxy resin, hardener, catalyst and reactive diluent were blended to form the epoxy resin mixture. The weight ratio of epoxy-to-hardener was 1:0.85 while the weight ratio of epoxy-to-catalyst was 100:1. The weight ratio of epoxy-to-diluent was 1:2. Thirdly, $Bi_{0.5}Sb_{1.5}Te_3$ powders and epoxy resin mixture were blended for 1 h with a mechanical stirrer and then ultrasonically dispersed for 15 min to obtain printable slurries. The optimized weight ratio of $Bi_{0.5}Sb_{1.5}Te_3$ powders and epoxy resin mixture was 3:1.

Fig. 1. FESEM image of ball-milled $Bi_{0.5}Sb_{1.5}Te_3$ powders.

2.2. Design of prototype flexible TE cooling device based on the (000*l*)-oriented $Bi_{0.5}Sb_{1.5}Te_3$/epoxy thick films

Fig. 2 schematically shows the procedure of fabricating prototype flexible TE cooling device based on the (000*l*)-oriented $Bi_{0.5}Sb_{1.5}Te_3$/epoxy thick films through the combination of brush-printing and hot-pressing curing processes. Besides the preparation of $Bi_{0.5}Sb_{1.5}Te_3$/epoxy slurries, the whole fabricating procedure still included flexible substrate pretreatment, template process, brush printing, drying, hot-pressing curing, and electrode deposition. The polyimide substrate with about 150 μm in thickness had been first plasma-cleaned and then was compactly covered with template. The $Bi_{0.5}Sb_{1.5}Te_3$/epoxy slurries were brush-printed and formed thick films with about 150 μm in thickness. The thick films were dried at 373 K for 30 min and then transferred into a homemade hot-pressing apparatus to have been cured at different temperatures (473 K, 523 K, 573 K and 623 K) and different hot-pressures (0 MPa, 2 MPa and 4 MPa) to yield compact TE thick films with (000*l*) preferential orientation. The TE legs were connected in series by depositing Al/Cu/Ni multilayer thin-film electrodes on the polyimide substrate and TE legs using a vacuum evaporation technique.

2.3. Measurements

Differential scanning calorimeter (DSC) and thermogravimetry (TG) curves of epoxy resin matrix and $Bi_{0.5}Sb_{1.5}Te_3$/epoxy composite were determined by a Netzsch STA449F3 integrative thermal analyzer in N_2 atmosphere in the range of 300–773 K at a heating ratio of 10 K/min. The constituent phases of all the $Bi_{0.5}Sb_{1.5}Te_3$/epoxy thick films were determined by X-ray diffraction (XRD, PANalytical X′ Pert PRO) using Cu K_α radiation (λ = 0.15418 nm). The microstructures were examined with a field emission scanning electron microscope (FESEM, Zeiss ULTRA-PLUS-43-13). The surface roughness and thickness of all the thick films were measured on a 500 μm × 500 μm area by employing 3D surface profilometer (NanoMap, 500LS) attached with a scanning probe image processor and analysis software. The density of the thick films was measured with the Archimedes method. Hall coefficient (R_H) and electrical resistivity (ρ) of the thick films were measured with van der Pauw method using an Accent 5500 Hall measurement system at room temperature. The μ_H and n were calculated according to the equations $n = 1/(eR_H)$ and $\mu_H = R_H/\rho$, where e is the charge of an electron. The in-plane electrical conductivity (σ) and Seebeck coefficient (α) were measured with the standard four-probe method (Sinkuriko, ZEM-3) in He atmosphere. The measurement error for σ and α is about ± 5%. The bending tests of the thick films were performed using a homemade bending test apparatus. The cooling performance of the prototype devices based on $Bi_{0.5}Sb_{1.5}Te_3$/epoxy thick films were measured by a homemade apparatus. Currents generated from a DC power supply (Gwinstek, GPD-2303S) were applied on the prototype device, and the temperatures of hot side and cold one of TE legs were monitored by two high accuracy resistance temperature detectors (RTD).

3. Results and discussion

3.1. Structural evolution of $Bi_{0.5}Sb_{1.5}Te_3$/epoxy thick films during hot-pressing curing process

To determine the temperatures of the curing reaction and decomposition of epoxy resin, the DSC and TG curves of the epoxy resin matrix and $Bi_{0.5}Sb_{1.5}Te_3$/epoxy composites were measured and the results are displayed in Fig. 3. The excess diluent was added into the $Bi_{0.5}Sb_{1.5}Te_3$/epoxy slurries in order to decrease the viscosity. From the DSC curve (solid line) of the epoxy resin matrix, it can be seen that the largest exothermic peaks occur nearby the range of 375–410 K, originating from the curing reaction between the epoxy resin and anhydride hardener catalyzed by imidazole derivative [25]. The endothermic peak

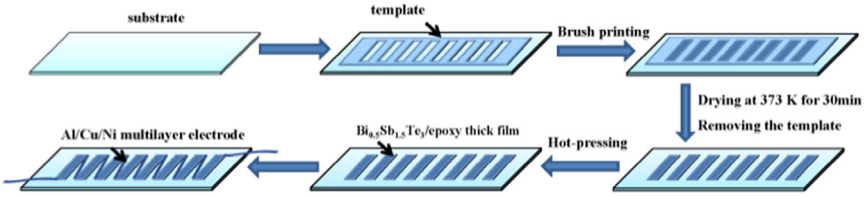

Fig. 2. Fabricating procedure of flexible prototype TE device with $Bi_{0.5}Sb_{1.5}Te_3$/epoxy thick films.

at about 540 K is related to the breakage of chemical bonds for small molecular groups such as -OH, -CH_2-, -CH_3, and C-O-C of epoxy resin [26]. The endothermic peak about 675 K is attributed to the breakage of epoxy resin. The carbonization reaction of aromatic rings for the epoxy resin occurred above 575 K [26]. From the DSC curve (dotted line) of $Bi_{0.5}Sb_{1.5}Te_3$/epoxy composites, all the exothermic peaks near the range of 375–410 K and endothermic peaks about 540 K, 675 K can be observed, although these peaks were significantly weakened as compared with those of the epoxy resin matrix due to the smaller weight percent of epoxy resin in the composites. In the TG curves of the epoxy resin (solid line) and $Bi_{0.5}Sb_{1.5}Te_3$/epoxy composites (dotted line), the small weight loss near the range of 510–575 K originates from the breakage of chemical bonds of small molecular groups of the epoxy resin, the big weight loss above 575 K is attributed to the loss of epoxy resin. According to the DSC and TG curves of the epoxy resin matrix and the $Bi_{0.5}Sb_{1.5}Te_3$/epoxy composites, the curing of epoxy resin occurred nearby the range of 375–410 K and the decomposition of epoxy network occurred above 575 K.

Fig. 4 shows XRD patterns of the $Bi_{0.5}Sb_{1.5}Te_3$/epoxy thick films cured under non-pressure at 623 K and under 4 MPa at different temperatures in the range of 473–623 K. All the diffraction peaks can be indexed to the standard diffraction data of $Bi_{0.5}Sb_{1.5}Te_3$ with JCPDS 49-1713, indicating that these thick films were composed of single-phase $Bi_{0.5}Sb_{1.5}Te_3$. It can be seen that the orientations of $Bi_{0.5}Sb_{1.5}Te_3$ grains in these thick films strongly depend on the pressure and curing temperatures. At the curing condition of 623 K, the diffraction intensities of (0006) reflections of the hot-pressed samples (under 623 K and 4 MPa) dramatically increased as compared with that of the non-pressure sample (623 K without pressure). In particular, the diffraction intensities of all the (000*l*) reflections of $Bi_{0.5}Sb_{1.5}Te_3$ grains for the $Bi_{0.5}Sb_{1.5}Te_3$/epoxy thick films were gradually increased with increasing the curing temperature. These evolution features imply that the (000*l*) orientations of $Bi_{0.5}Sb_{1.5}Te_3$ grains were gradually increased with increasing the curing temperatures under the same pressure. Therefore, it is very clear that the hot-pressing treatment can dramatically improve the (000*l*) preferential orientation of $Bi_{0.5}Sb_{1.5}Te_3$ grains in the thick films during the curing process.

To quantitatively investigate the effect of the hot-pressing curing treatment on the preferential orientation of $Bi_{0.5}Sb_{1.5}Te_3$ grains, the orientation factors (*F*) of the $Bi_{0.5}Sb_{1.5}Te_3$/epoxy thick films were calculated with Lotgering's method [27].

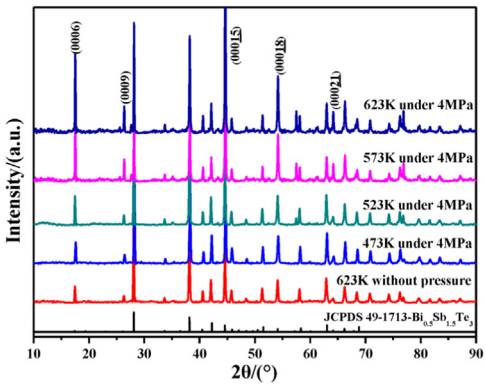

Fig. 4. XRD patterns of the $Bi_{0.5}Sb_{1.5}Te_3$/epoxy thick films cured under non-pressure at 623 K and under 4 MPa and different temperatures.

$$F(X) = (P - P_0)/(1 - P_0) \quad (1)$$

$$P = \Sigma I(X)/\Sigma I(hkil)\ P_0 = \Sigma I_0(X)/\Sigma I_0(hkil) \quad (2)$$

where $\Sigma I(X)$, $\Sigma I_0(X)$, $\Sigma I(hkil)$, and $\Sigma I_0(hkil)$ are the sum of the intensities of the *X* and (*hkil*) reflections for the oriented sample and the non-oriented one, respectively; *P* and P_0 is the ratio of the sums for the oriented sample and the non-oriented one, respectively. The *F* values of (000*l*) diffractions were 0.06, 0.09, 0.16, 0.31 and 0.43 for the thick films cured under non-pressure at 623 K and hot-pressing at 473 K, 523 K, 573 K, and 623 K, respectively. These results clearly reveal that the preferential orientations along the (000*l*) plane of the thick films were significantly increased as increasing the curing temperature and pressure. Under the curing condition of 623 K, the *F* value dramatically increased from 0.06 for the non-pressure sample to 0.43 for the hot-pressing sample, increased by 617%. Fig. 5 shows FESEM images of cross sections of $Bi_{0.5}Sb_{1.5}Te_3$/epoxy thick films fabricated at the curing temperatures of 473 K, 523 K, 573 K, and 623 K. These images indicate that all the thick films consist of layered $Bi_{0.5}Sb_{1.5}Te_3$ particles and epoxy resin. The grain size of $Bi_{0.5}Sb_{1.5}Te_3$ particles is in the range of 1–10 μm and the epoxy resin was distributed among $Bi_{0.5}Sb_{1.5}Te_3$ particles. In the thick film cured at 473 K, most of $Bi_{0.5}Sb_{1.5}Te_3$ particles are perpendicular or tilted to the substrate though a few $Bi_{0.5}Sb_{1.5}Te_3$ particles are parallel to the substrate. As the curing temperature increases from 473 K to 623 K, $Bi_{0.5}Sb_{1.5}Te_3$ particles parallel to the

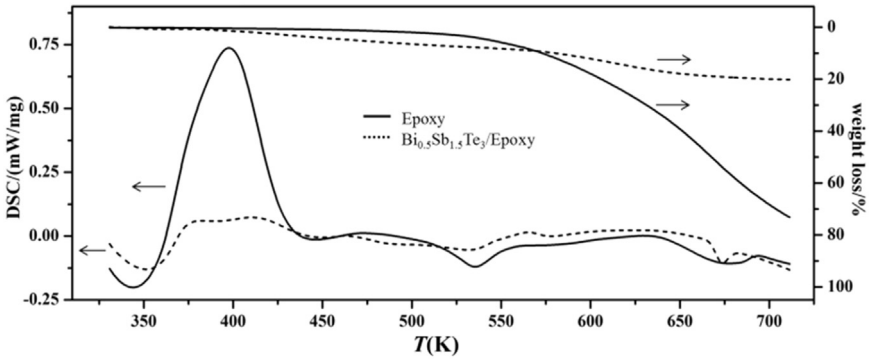

Fig. 3. DSC and TG curves of epoxy resin matrix and $Bi_{0.5}Sb_{1.5}Te_3$/epoxy composite.

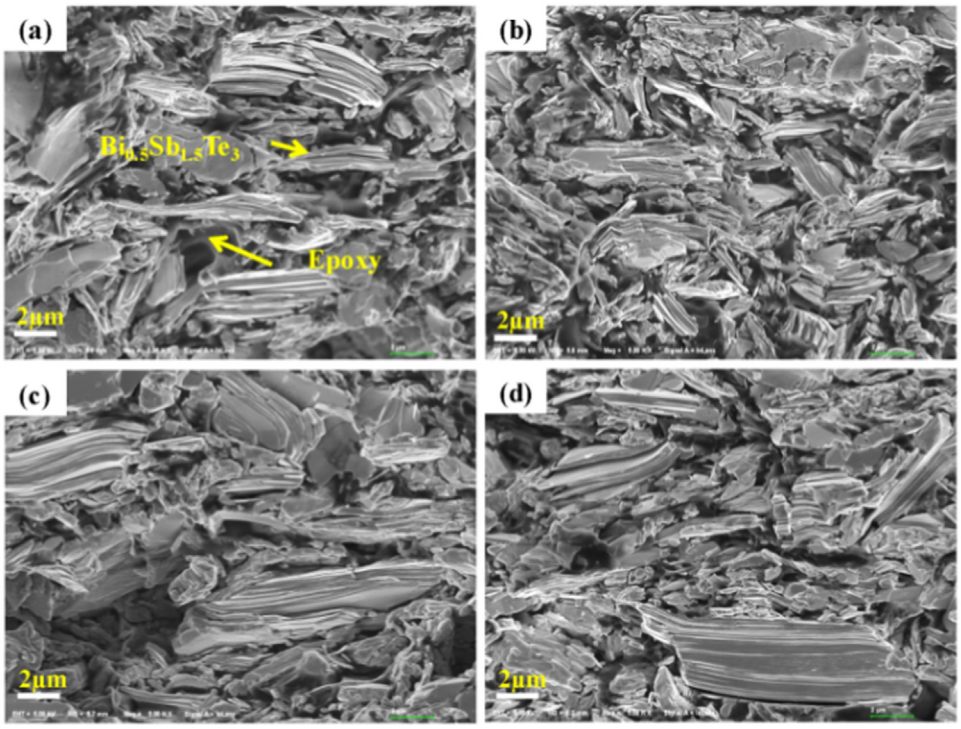

Fig. 5. FESEM images of cross sections of $Bi_{0.5}Sb_{1.5}Te_3$/epoxy thick films fabricated at different curing temperatures. (a) 473 K, (b) 523 K, (c) 573 K, (d) 623 K.

substrate become more and more, indicating that the (000*l*) preferential orientation of $Bi_{0.5}Sb_{1.5}Te_3$ particles was gradually enhanced in the thick films. This is in good agreement with the result from XRD analysis. The enhanced (000*l*) preferential orientation of $Bi_{0.5}Sb_{1.5}Te_3$ particles was mainly attributed to the beneficial effect of hot-pressing curing treatment. The applied pressure causes the random $Bi_{0.5}Sb_{1.5}Te_3$ particles to be rearranged along the (000*l*) orientation during the curing process. In addition, $Bi_{0.5}Sb_{1.5}Te_3$ fine particles were recrystallized and grown along the (000*l*) plane of $Bi_{0.5}Sb_{1.5}Te_3$ particles as increasing the curing temperature, resulting in a more stable system according to the energy minimum principle [28]. This is due to that the (000*l*) plane has the lowest surface energy in the $Bi_{0.5}Sb_{1.5}Te_3$ system. It is easy to understand that the (000*l*)-oriented rearrangement of $Bi_{0.5}Sb_{1.5}Te_3$ particles can dramatically reduce various defects such as interstitial pores and stacking faults, and remarkably increase the density of $Bi_{0.5}Sb_{1.5}Te_3$/epoxy thick films [29]. The growth of $Bi_{0.5}Sb_{1.5}Te_3$ fine particles also causes a part of layered $Bi_{0.5}Sb_{1.5}Te_3$ particles to be contacted with each other and to form conductive channels [30]. All these evolutions are responsible for the significant enhancement in the electrical transport properties of the $Bi_{0.5}Sb_{1.5}Te_3$/epoxy thick films. In addition, all the IR absorption peaks assigned to epoxy resin with methylhexahydrophthalic anhydride are appeared in the FTIR spectra of $Bi_{0.5}Sb_{1.5}Te_3$/epoxy composites having been cured in the temperature range of 473–623 K, indicating that the epoxy resin still exist in all the cured thick films.

Fig. 6 shows the surface 3D images of $Bi_{0.5}Sb_{1.5}Te_3$/epoxy thick films fabricated at the curing temperatures of 473 K, 523 K, 573 K and 623 K. The surface roughness of the thick film cured at 473 K is the largest and reaches 296 nm. As increasing the curing temperature, the surface roughness is remarkably decreased to 259 nm, 135 nm, and 85 nm for the thick films cured at 523 K, 573 K, and 623 K, respectively. The significant decrease in the surface roughness of the thick films originates from the re-arrangement of $Bi_{0.5}Sb_{1.5}Te_3$ particles along the (000*l*) orientation. This is in good accordance with the results from XRD and FESEM analysis.

A schematic densification process of the $Bi_{0.5}Sb_{1.5}Te_3$/epoxy thick films during the hot-pressing curing process is shown in Fig. 7. A hot-pressing apparatus was designed to dimensionally match with the thick films and it provided maximum pressure about 4 MPa. The hot-pressing apparatus provided the necessary contact force on the surface of the thick films and causes the randomly oriented $Bi_{0.5}Sb_{1.5}Te_3$ particles to be rearranged along the (000*l*) orientation during the curing process. The detailed mechanism of re-arrangement of $Bi_{0.5}Sb_{1.5}Te_3$ particles during the hot-pressure curing process was reported by our previous work [29].

In order to further reveal the effects of the hot-pressing curing process on the $Bi_{0.5}Sb_{1.5}Te_3$/epoxy thick films, the thick films were cured at 0 MPa, 2 MPa, 3 MPa and 4 MPa at 623 K for 10 h. Fig. 8 shows FESEM images of the cross sections of thick films cured under non-pressure and different pressures. As shown in Fig. 8**a**, large cracks and voids were found in the thick film cured under non-pressure, which were a consequence of volatilization of small molecular in the epoxy system during the curing process. Benefitting from the hot-pressing curing treatment, cracks and most of voids were disappeared and the density of the thick films (shown in Table 2) was significantly improved due to the decrease in thickness, as shown in Fig. 8**c** and **e**. In particular, the $Bi_{0.5}Sb_{1.5}Te_3$ particles were randomly distributed in the thick films under non-pressure as shown in Fig. 8**b.** With applying 2 MPa and 4 MPa pressures, the (000*l*) preferential orientation of $Bi_{0.5}Sb_{1.5}Te_3$ particles was enhanced. As a result, the densification of the thick films was improved.

Fig. 9 shows the surface 3D images of $Bi_{0.5}Sb_{1.5}Te_3$/epoxy thick films cured under non-pressure and different pressures. The surface roughness is 1138 nm for the non-pressure thick films. Compared with the non-pressure thick film, the surface roughness of all the hot-pressed thick films had been significantly reduced and was only 132 nm and 85 nm for the thick films cured under the pressure of 2 MPa and 4 MPa, respectively. The significant decrease in the surface roughness is attributed to the re-arrangement of $Bi_{0.5}Sb_{1.5}Te_3$ particles along the (000*l*) orientation, thus forming much smoother surfaces.

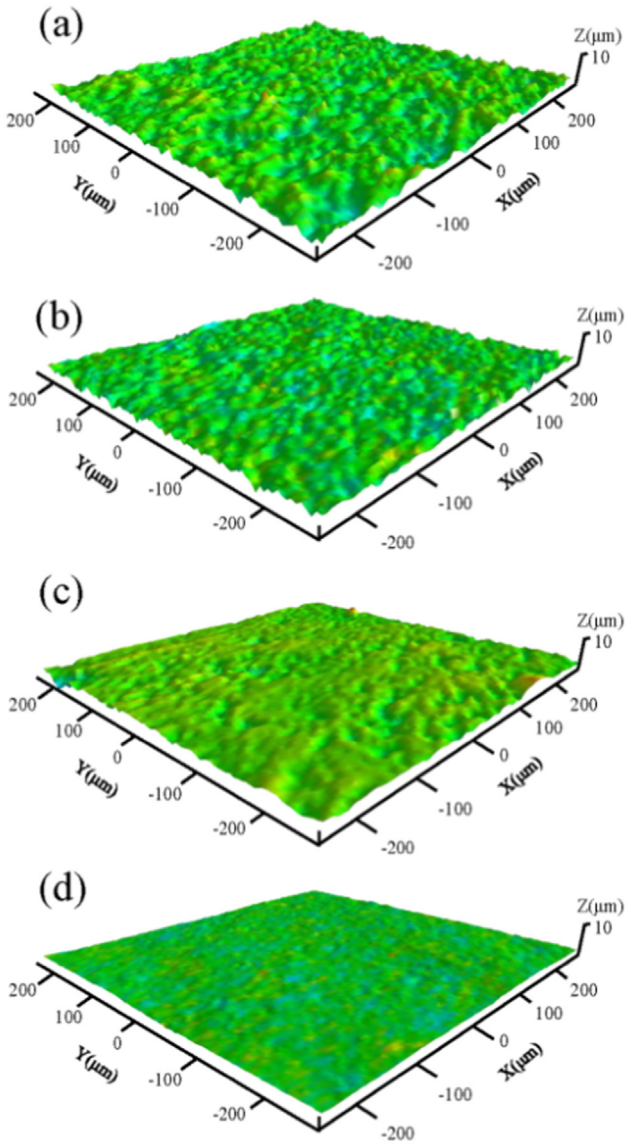

Fig. 6. Surface 3D images of $Bi_{0.5}Sb_{1.5}Te_3$/epoxy thick films fabricated at different curing temperatures. (a) 473 K, (b) 523 K, (c) 573 K, (d) 623 K.

3.2. Beneficial effects of hot-pressing curing on transport properties of $Bi_{0.5}Sb_{1.5}Te_3$/epoxy thick films

The room-temperature electrical transport properties of $Bi_{0.5}Sb_{1.5}Te_3$/epoxy thick films cured at different temperatures in the range of 473–623 K under 4 MPa pressure are listed in Table 1. The positive Hall coefficient (R_H) for all the thick films indicated that the majority of carriers were holes. The *p*-type conduction feature was consistent with the corresponding bulk materials [31,32]. The thick film cured at 473 K showed very low Hall mobility of only 1.6 $cm^2\ V^{-1}\ s^{-1}$ in spite of remaining relatively high carrier concentration around $1.9 \times 10^{19}\ cm^{-3}$, which finally led to low σ and power factor ($\alpha^2\sigma$). The poor electrical properties are attributed to the poor electrical contact between adjacent $Bi_{0.5}Sb_{1.5}Te_3$ particles. The carrier concentration of the thick films slightly decreased from $1.93 \times 10^{19}\ cm^{-3}$ at the curing temperature of 473 K to $1.62 \times 10^{19}\ cm^{-3}$ at the curing temperature of 623 K, suggesting that the antisite defects of $Bi_{0.5}Sb_{1.5}Te_3$ particles slightly decreased with increasing the curing temperature, benefiting from the increased donor-like effect [33,34]. It is worth noting that the Hall mobility of thick films dramatically increased from 1.6 $cm^2\ V^{-1}\ s^{-1}$ for the thick film cured at 473 K to 44.13 $cm^2\ V^{-1}\ s^{-1}$ for the thick film cured at 623 K, increased by 2658%. The remarkable increase in the Hall mobility is attributed to the (000*l*) preferential orientation and the improved electrical contact between $Bi_{0.5}Sb_{1.5}Te_3$ particles. Our previous theoretical and experimental results had also proved that the (000*l*) orientation of $Bi_{0.5}Sb_{1.5}Te_3$ particles might greatly increase the mobility [29].

Fig. 10 shows the temperature dependence of electrical conductivity, Seebeck coefficient, and power factor of the $Bi_{0.5}Sb_{1.5}Te_3$/epoxy thick films fabricated at different curing temperatures in the range of 473–623 K under 4 MPa pressure. It is worth noting that the σ, α, and $\alpha^2\sigma$ simultaneously increased with increasing the curing temperature. The σ and α of the thick film cured at 623 K were the largest at 300 K and reached $1.15 \times 10^4\ S\ m^{-1}$ and 270 $\mu V\ K^{-1}$. As a result, the largest $\alpha^2\sigma$ reached 0.84 $mW\ K^{-2}\ m^{-1}$, increased by 2198%, 27%, and 3552% as compared with those of the thick film cured at 473 K, respectively. The σ of the thick film cured at 473 K increased slightly in the range of 300–460 K as shown in Fig. 10**a**. However, for the thick films cured at 523 K, 573 K and 623 K, the σ first decreased and then slightly increased above 400 K, similar with the metallic transport behavior observed on the bulk $Bi_{0.5}Sb_{1.5}Te_3$ materials [35]. The difference is mainly due to the (000*l*) preferential orientation and enhanced contact of $Bi_{0.5}Sb_{1.5}Te_3$ particles. For the thick films cured at 473 K, the contact of $Bi_{0.5}Sb_{1.5}Te_3$ particles was loose, the main conductive mechanism was tunnel conductivity, in which the molecular thermal vibration caused the electron migration through a conductive tunnel between the adjacent conductive particles under the electric field [36]. This effect was enhanced when the temperature rose, thus the σ increased with increasing the temperature. For the thick films cured at 523, 573 and 623 K, the (000*l*) preferential orientation and compact contact of $Bi_{0.5}Sb_{1.5}Te_3$ particles formed conductive network due to the decrease in the thickness and the increase in the densities of the $Bi_{0.5}Sb_{1.5}Te_3$/epoxy thick films as increasing curing temperature, thus exhibiting metallic transport properties. The lower σ at low temperature is due to the strong electron-phonon scattering. The increase in the σ at high temperature is a consequence of bipolar effect. The σ at 300 K greatly increased from $0.5 \times 10^3\ S{\cdot}m^{-1}$ for the thick film cured at 473 K to $11.5 \times 10^3\ S\ m^{-1}$ for the thick film cured at 623 K. The remarkable increment is attributed to the compact grain contact induced by the (000*l*) orientation of $Bi_{0.5}Sb_{1.5}Te_3$ particles. The positive α as shown in Fig. 10**b** is indicative of *p*-type conduction behavior, which is consistent with the Hall measurements. With increasing the

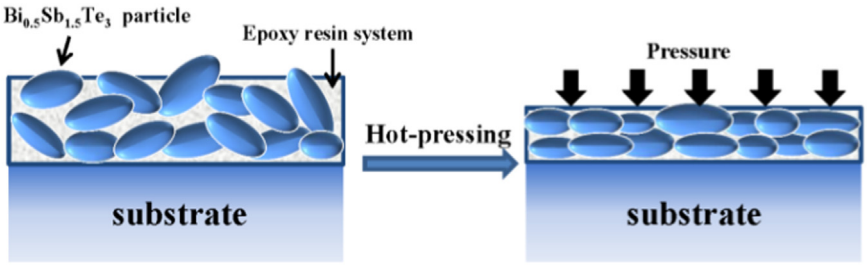

Fig. 7. Schematic densification process of $Bi_{0.5}Sb_{1.5}Te_3$/epoxy thick films during the hot-pressing curing process.

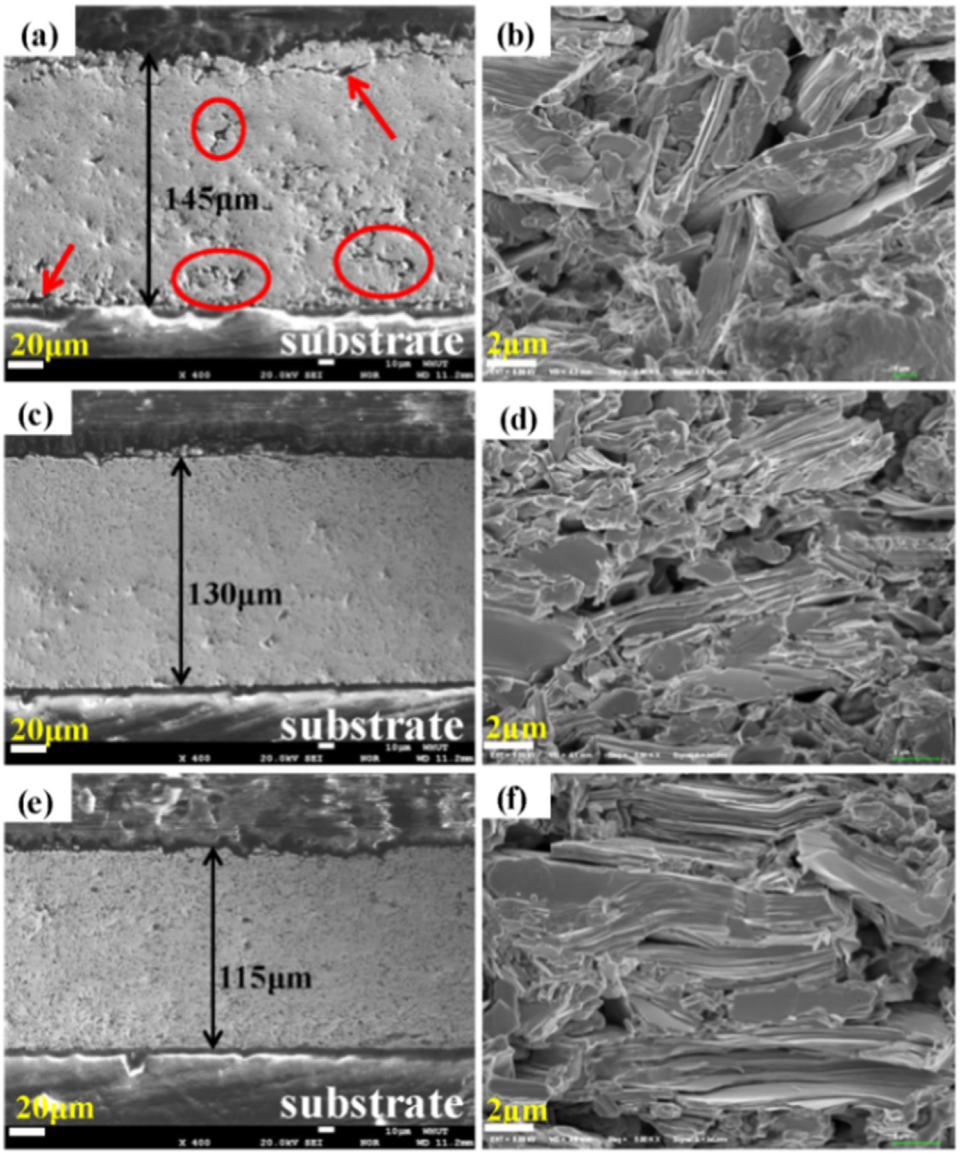

Fig. 8. FESEM images of cross sections of $Bi_{0.5}Sb_{1.5}Te_3$/epoxy thick films cured under non-pressure and different pressures: (a, b) 0 MPa, (c,d) 2 MPa, and (e, f) 4 MPa.

temperature, the α value first increased and then decreased. The increased α is related to the strong electron scattering from the boundaries between adjacent $Bi_{0.5}Sb_{1.5}Te_3$ particles for the thick films cured at low temperatures, but to the strong electron-phonon scattering for the thick films cured at high temperatures. The reduction in the α above 350–390 K is a consequence of intrinsic excitation. Note that the gradual increase in α with increasing the curing temperature in the range of 473–623 K is related to the changes in the carrier concentration and the electron scattering mechanism from the boundary scattering to electron-phonon one.

By optimizing the curing temperature, the $\alpha^2\sigma$ values of $Bi_{0.5}Sb_{1.5}Te_3$/epoxy thick films were remarkably improved in the whole temperature range. The highest $\alpha^2\sigma$ value of 0.84 mW K^{-2} m^{-1} was obtained at 300 K for the thick film cured at 623 K and 4 MPa. The excellent electrical transport properties originate from the simultaneous increases in σ and α induced by the (000*l*) preferential orientation and compact contact of $Bi_{0.5}Sb_{1.5}Te_3$ particles.

Fig. 11 shows the temperature dependence of electrical conductivity, Seebeck coefficient, and power factor of $Bi_{0.5}Sb_{1.5}Te_3$/epoxy thick films cured at 623 K under non-pressure and different pressures. The similar temperature dependence of the σ indicates the metallic transport behavior. The σ values of $Bi_{0.5}Sb_{1.5}Te_3$/epoxy thick films cured under hot-pressing conditions were much higher than those of non-pressure films in the range of 300–450 K, while the α did not show a noticeable change. The thick film cured under 4 MPa pressure showed an increase of 224% in the σ as compared with that of the non-pressure thick film. This is reasonably interpreted in terms of the microstructure changes during the hot-pressing curing process. Therefore, the $\alpha^2\sigma$ of hot-pressed thick films dramatically increased in the whole temperature range. The room-temperature electrical transport properties of $Bi_{0.5}Sb_{1.5}Te_3$/epoxy thick films cured under non-pressure and different pressures are listed in Table 2. It can be seen that the Hall mobility was significantly increased as the pressure increased. This is attributed to the significant enhancement in (000*l*) preferential orientation and the improvement in grain contact of $Bi_{0.5}Sb_{1.5}Te_3$ particles. Note that the α of the hot-pressed thick films kept almost unchanged in spite of large improvement in σ, which is mainly due to the improved Hall mobility. As a result, the $\alpha^2\sigma$ is remarkably improved through the hot-pressing curing treatment, and the highest $\alpha^2\sigma$ of $Bi_{0.5}Sb_{1.5}Te_3$/epoxy thick films reached 0.84 mW K^{-2} m^{-1} at 300 K cured under the pressure of 4 MPa

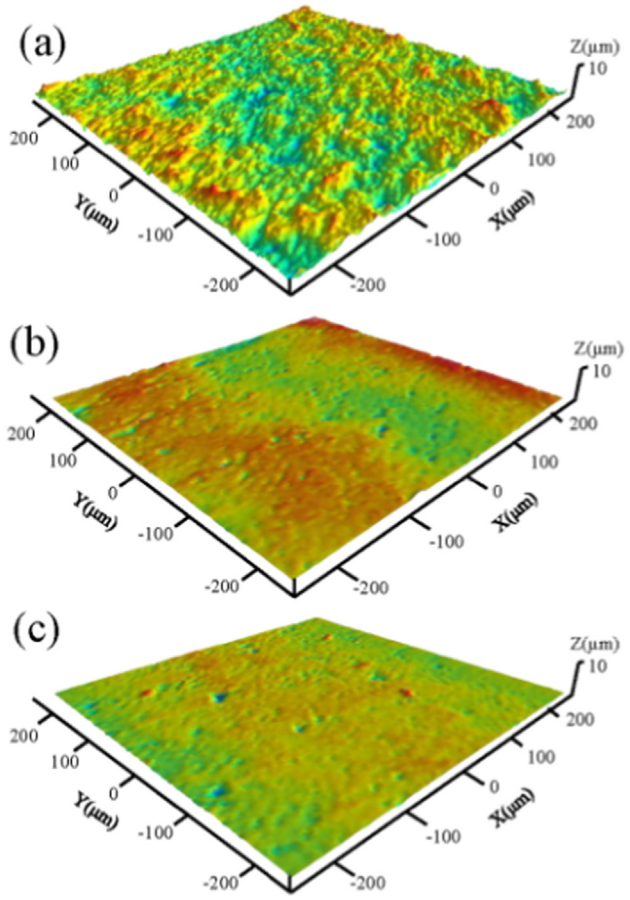

Fig. 9. 3D images of the surface of $Bi_{0.5}Sb_{1.5}Te_3$/epoxy thick films cured under non-pressure and different pressures: (a) 0 MPa, (b) 2 MPa, (c) 4 MPa.

at 623 K, increased by 250% as compared with that of the cured thick film without applying pressure. Fig. 12 shows the temperature dependence of the power factor of Bi_2Te_3/epoxy thick films fabricated by different printing methods. It can be seen that the $\alpha^2\sigma$ values of our hot-pressed thick films are much higher than all the data of non-pressure thick films reported by different groups [20,22,37,38], showing an increment about 223% as compared to that of the Bi_2Te_3 + 1 wt%Se/epoxy thick films with the highest $\alpha^2\sigma$ of 0.26 mW K^{-2} m^{-1} [22]. The remarkable enhancement in the $\alpha^2\sigma$ for this work demonstrates that the hot-pressing curing treatment is an effective approach to fabricate high-performance Bi_2Te_3/epoxy thick films. The (000*l*) preferential orientation and the high density, which were formed during the hot-pressing curing process, should be responsible for the excellent electrical transport properties of the Bi_2Te_3/epoxy thick films.

3.3. Cooling performance of prototype flexible device based on $Bi_{0.5}Sb_{1.5}Te_3$/epoxy thick films

To minimize the interfacial thermal/electrical resistance between the TE thick films and electrodes, and make the electrodes as stable as possible, we had designed a transition layer of Ni between Cu and thick film to decrease the lattice mismatch between Cu and Bi_2Te_3, and at the meantime added a protective layer on the surface of electrode to prevent Cu electrode from oxidization. The low interface resistance and excellent anti-oxidation of the Al/Cu/Ni multilayer thin-film electrode has been reported in our previous work [39]. As shown in Fig. 13, a prototype flexible thick film device had been designed and successfully fabricated on a flexible polyimide substrate, which consists of $Bi_{0.5}Sb_{1.5}Te_3$/epoxy thick films with the (000*l*) preferential orientation and Al/Cu/Ni multilayer thin film electrodes with low interface resistance and excellent anti-oxidation. $Bi_{0.5}Sb_{1.5}Te_3$/epoxy thick film legs were in-series connected by Al/Cu/Ni multilayer thin-film electrodes. The prototype flexible device was about 260 μm in height and 60 mm in length. The total resistance was about 40 Ω.

Fig. 14 shows the rates of resistances (R/R_0) before and after bending test with different bending radius and cycle times. The initial internal resistance (R_0) of the device was 40 Ω. The internal resistance (R) is almost unchanged when the bending radius was gradually decreased from 90 mm to 10 mm as shown in Fig. 14**a**, and starts to rapidly increase when the bending radius decreased from 10 mm to 8 mm. The TE legs were cracked when the bending radius was less than 5 mm. To further investigate the flexible thermoelectric cooling device, the R is measured during the cycling bending test under the condition of bending radius between 20 mm and 90 mm. It is noteworthy that the R is almost no change when the cycle times are less than 2500, and increase due to the appearance of microcracks in the TE legs. When the

Table 1
Density and room-temperature electrical properties of $Bi_{0.5}Sb_{1.5}Te_3$/epoxy thick films fabricated at different curing temperatures *T*.

T	Density (g cm^{-3})	R_H (10^{-1} cm^3 C^{-1})	*n* (10^{19} cm^{-3})	μ_H (cm^2 V^{-1} s^{-1})	σ (10^3 S m^{-1})	α (μV K^{-1})	$\alpha^2\sigma$ (mW K^{-2} m^{-1})
473 K	3.73	3.23	1.93	1.62	0.5	213	0.023
523 K	4.28	3.59	1.74	12.75	3.55	258	0.24
573 K	4.62	3.66	1.71	26.32	7.19	263	0.50
623 K	4.96	3.84	1.62	44.13	11.5	270	0.84

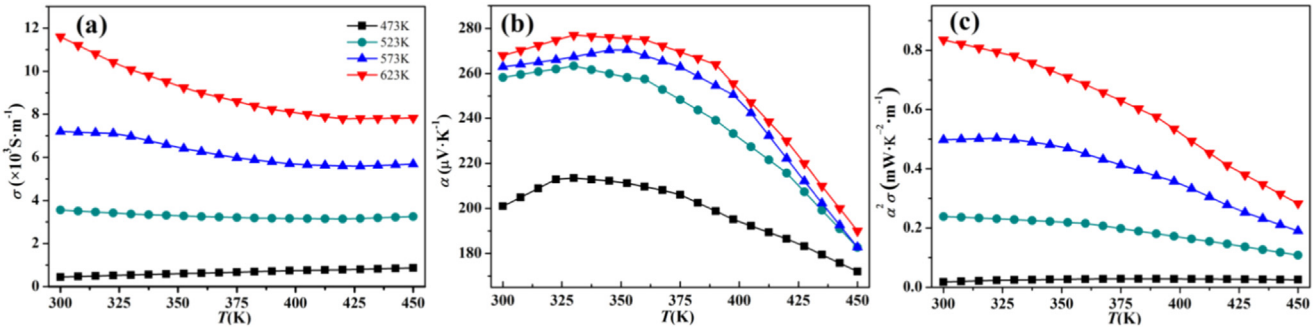

Fig. 10. Temperature dependence of (a) electrical conductivity, (b) Seebeck coefficient, and (c) power factor for $Bi_{0.5}Sb_{1.5}Te_3$/epoxy thick films fabricated at different curing temperatures.

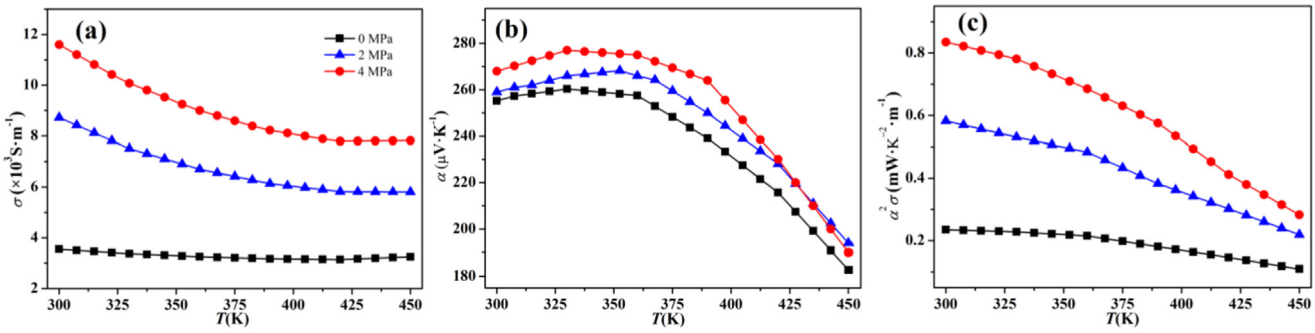

Fig. 11. Temperature dependence of (a) electrical conductivity, (b) Seebeck coefficient, and (c) power factor of $Bi_{0.5}Sb_{1.5}Te_3$/epoxy composite thick films cured under non-pressure and different pressures.

Table 2
Density and room-temperature electrical transport properties of $Bi_{0.5}Sb_{1.5}Te_3$/epoxy thick films cured under non-pressure and different pressures.

Sample	Density (g cm^{-3})	R_H (10^{-1} cm^3·C^{-1})	n (10^{19} cm^{-3})	μ_H (cm^2 V^{-1} s^{-1})	σ (10^3 S m^{-1})	α (μV K^{-1})	$\alpha^2\sigma$ (mW K^{-2} m^{-1})
$Bi_{0.5}Sb_{1.5}Te_3$(0 MPa)	3.60	3.79	1.65	13.45	3.55	258	0.24
$Bi_{0.5}Sb_{1.5}Te_3$(2 MPa)	4.58	3.83	1.63	33.97	8.87	260	0.58
$Bi_{0.5}Sb_{1.5}Te_3$(4 MPa)	4.95	3.86	1.62	44.13	11.49	270	0.84

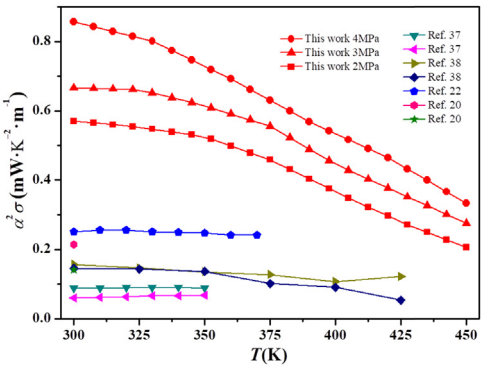

Fig. 12. Temperature dependence of the power factor of Bi_2Te_3 based TE material/epoxy thick films fabricated by different printing methods.

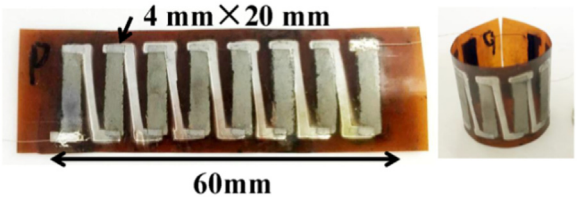

Fig. 13. A prototype flexible device consisting of $Bi_{0.5}Sb_{1.5}Te_3$/epoxy thick films, Al/Cu/Ni multilayer thin-film electrodes, and a polyimide substrate.

cycle times reach 4700, the TE legs were cracked and the resistance was rapidly increased, as a result, the device is in complete failure.

To evaluate the cooling performance of the prototype device, the temperatures of hot side (T_h) and cold one (T_c) of the legs had been measured under different applied currents (I). Fig. 15 shows the time dependences of T_h and T_c under different I. As a current of 0.02 A was applied, the T_h increased rapidly in the first 50 s and then decreased slightly, while the T_c decreased slowly during the whole measurement process. The T_c was decreased about 0.7 K. The maximum temperature difference (ΔT_{max}) between the hot and cold sides was about 1.4 K. When the I was 0.06 A, the T_h increased from 300 K to 307.2 K while the T_c increased from 300 K to 301 K in the first 50 s, and then the T_h and T_c were unchanged in the following measurement process, thus establishing a stable ΔT_{max} of about 6.2 K. When the I was more than 0.06 A, the ΔT_{max} was about 11.7 K for I = 0.10 A, 13.1 K for I = 0.14 A and 17.9 K for I = 0.18 A, respectively. However, the T_h and T_c were gradually increased with increasing the time due to Joule heat effect induced by the internal resistance of the device. According to the thermodynamic analysis of TE cooling device [40,41], the thermal energy in the device depends on several different effects, such as thermal energy from Peltier effect, thermal conduction energy from Fourier effect, and Joule thermal energy from the internal resistance of the device. When the thermal energy from Peltier effect was greater than those from Fourier effect and Joule heat effect, the T_c was decreased, as shown in Fig. 15**(a)**. However, when a large electrical current was applied, the thermal from Fourier effect and Joule heat effect, as a consequence, energy from Peltier effect was not enough to offset those the T_c was increased and the ΔT_{max} gradually decreased, as shown in Fig. 15**(c)–(e)**. Therefore, the proper working current is essential to establish a stable temperature difference on the TE cooling devices. The stable temperature difference of the prototype devices was about 6.2 K under the working electric current of 0.06 A. Table 3 summarizes the cooling performances and corresponding working conditions of Bi_2Te_3-based film TE devices reported by us and different groups [3,4,10,18,42–46]. As shown in Table 3, the temperature differences of Bi_2Te_3-based film TE devices reported by other groups is much lower than 6.2 K of the $Bi_{0.5}Sb_{1.5}Te_3$/epoxy thick film prototype device. The temperature difference of our prototype device was increased by about 24% as compared to the highest temperature difference of 5 K evaluated with infrared image microscopy [43]. The excellent cooling performance of our prototype device originates from the excellent electrical transport properties of $Bi_{0.5}Sb_{1.5}Te_3$/epoxy thick films with the (000l) preferential orientation of $Bi_{0.5}Sb_{1.5}Te_3$ grains and Al/Cu/Ni multilayer thin-film electrode. This work demonstrates that our flexible prototype device has potential use in the in-plane heat dissipation of various electronic systems such as chips, mobile phone, and tablet computer. However, our $Bi_{0.5}Sb_{1.5}Te_3$/epoxy prototype devices cannot produce a stable temperature difference when the I is more than 0.06 A because of large Joule heat induced by the internal resistance. The further work will focus on decreasing the internal resistance and enlarging the temperature difference by designing a new hot-pressing apparatus able to provide higher pressure, and meanwhile optimizing the ratio of $Bi_{0.5}Sb_{1.5}Te_3$ and epoxy.

Both temperature difference and T_c are important parameters to evaluate the cooling performance of a TE device. Ideally, the T_c will gradually decrease or keep unchangeable during the TE device while

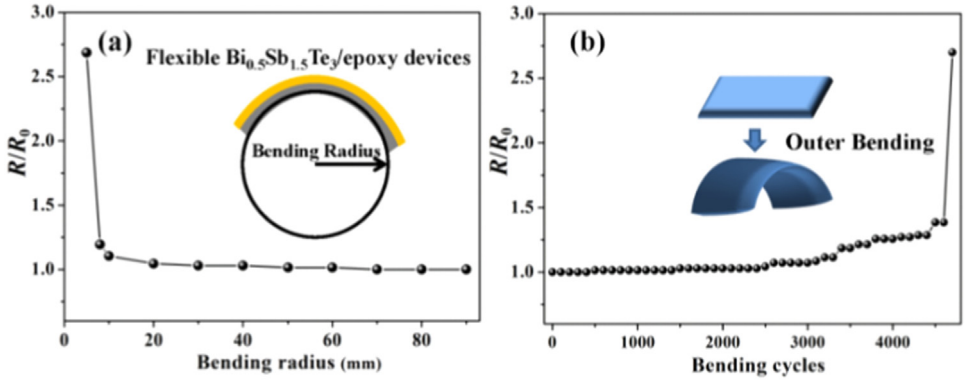

Fig. 14. Bending tests of flexible $Bi_{0.5}Sb_{1.5}Te_3$/epoxy device according to (a) bending radius and (b) bending cycles.

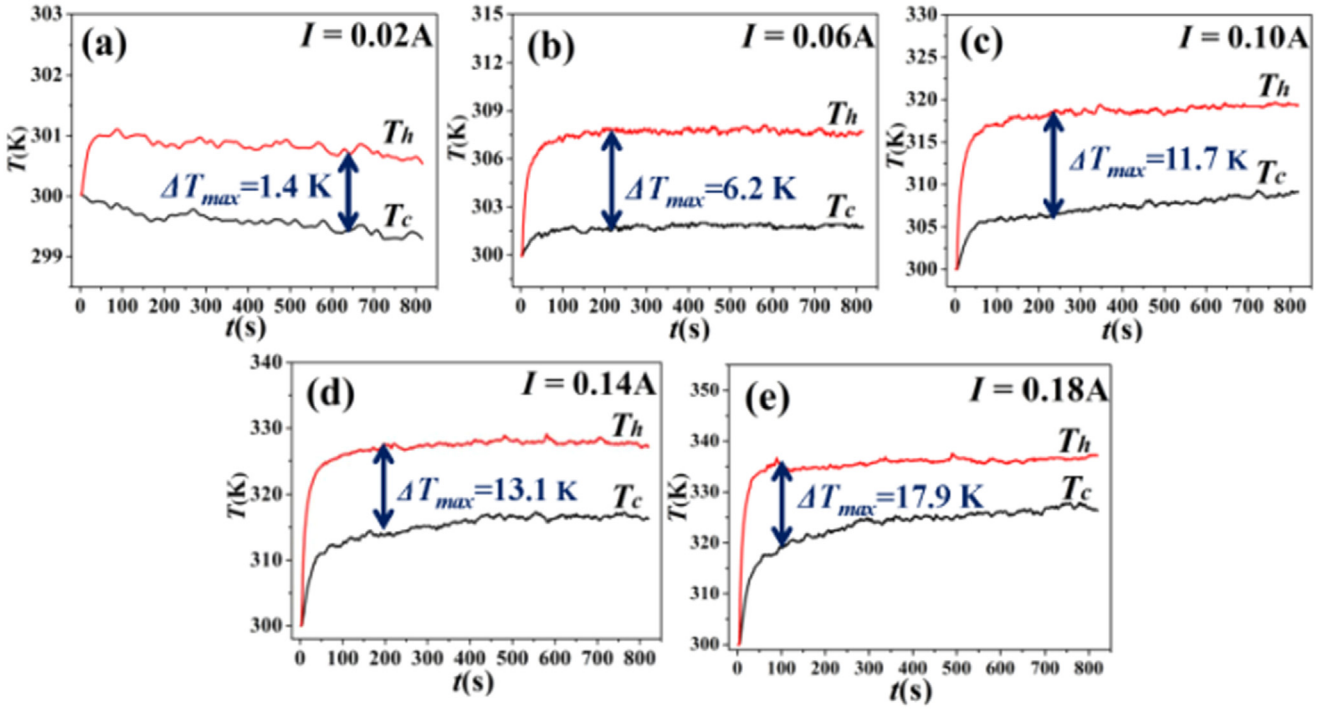

Fig. 15. Cooling performance of prototype device based on $Bi_{0.5}Sb_{1.5}Te_3$/epoxy thick films with the (000*l*) preferential orientation.

Table 3
Comparison of cooling performance and corresponding working conditions of Bi_2Te_3-based film TE devices reported by different groups.

Materials	Devices	Electrode	TE film Thickness(μm)	$\alpha^2\sigma$ (mW K^{-2} m^{-1})	R (Ω)	I (mA)	ΔT (K)	Ref.
p-$Bi_{0.5}Sb_{1.5}Te_3$/epoxy	8 single *p*-type	Al/Cu/Ni	110	0.84	40	60	6.2	This work
p-$Bi_{0.5}Sb_{1.5}Te_3$, *n*-$Bi_2Te_{2.7}Se_{0.3}$	3 pairs *p-n*	Ag	~ 5	0.06, 0.16	–	–	3.2	[10]
p-$Bi_{0.5}Sb_{1.5}Te_3$, *n*-$Bi_2Te_{2.7}Se_{0.3}$	4 pairs *p-n*	Cu	150	0.15, 0.24	100	100	2.3	[18]
p-Sb_2Te_3	single *p*-type	Au	0.1	–	–	30	1.8	[42]
n-Bi_2Te_3/*p*-Sb_2Te_3	21 layers *p/n*	Au	0.1	–	–	5	3	[3]
p-Bi_2Te_3/Sb_2Te_3, *n*-Bi_2Te_3/Bi_2Te_2Se	10240 pairs *p-n*	Au	0.31	0.14, 0.4	–	175	0.7	[4]
p-Sb_2Te_3, *n*-Bi_2Te_3	4 pairs *p-n*	Ni/Al	10	0.49, 0.86	–	4	5	[43]
p-Sb_2Te_3, *n*-Bi_2Te_3	126 pairs *p-n*	Ni/Au	20	–	33	111	2	[44]
p-Sb_2Te_3, *n*-Bi_2Te_3	60 pairs *p-n*	Cr/Au/Ti/Pt	4.5	0.3, 0.15	51	23	1.3	[45]
p-Sb_2Te_3, *n*-Bi_2Te_3	200 pairs *p-n*	Cr/Au	8	0.08, 0.3	–	200	1.2	[46]

the temperature difference should be as big as possible. Namely, the bigger the temperature difference is and the lower the T_c is, the better the cooling performance of TE device is. However, due to the Joule heat induced by the internal resistance, the T_c must be raised when the working current increase enough to be big. Therefore, one generally selects a critical current, which guarantees the T_c to be almost unchangeable, as the maximum working current of TE device to obtain the maximum temperature different. Based on these considerations, the current of 0.06 A is just the critical current for the TE device reported by us that may establish a stably maximum temperature different of about 6.2 K. We ensured that the temperature difference of 6.2 K reported in this work is the best result for flexible thick films TE device based on organic/inorganic composite TE materials through thermocouple thermometers technology. We will investigate the errors of temperature

measurements through infrared image microscopy and thermocouple thermometers in the follow-up work and ensure whether our result is also the best for infrared image microscopy.

4. Conclusions

$Bi_{0.5}Sb_{1.5}Te_3$/epoxy thick films with (000*l*) preferential orientation and excellent electrical transport properties have been fabricated through a simple and efficient method by the combination of brush-printing and hot-pressing processes. It is discovered that the curing temperature and hot pressure play a vital role in improving the microstructure and electrical transport properties. Optimizing the curing temperature and pressure led to significant enhancements in the (000*l*) preferential orientation and densification, and remarkable decrease in surface roughness and defects. Benefiting from these evolutions in preferential orientations and defects, $Bi_{0.5}Sb_{1.5}Te_3$/epoxy thick films exhibited remarkably improved carrier mobility, electrical conductivity, and power factor. The highest power factor reached 0.84 mW K^{-2} m^{-1} at 300 K for $Bi_{0.5}Sb_{1.5}Te_3$/epoxy thick film cured under 623 K and 4 MPa, increased by 250% and 223% as compared with that of our non-pressure thick film and the highest value reported by other groups, respectively. A prototype flexible cooling device was fabricated with the (000*l*)-oriented $Bi_{0.5}Sb_{1.5}Te_3$/epoxy thick films. The cooling performance of the prototype devices was evaluated under different applied currents. The stable temperature difference of the prototype devices is up to 6.2 K under the working current of 0.06 A, increased about 24% as compared to the highest value of 5 K reported by other groups. This work demonstrates that the hot-pressing curing process provides an effective approach to fabricate high-performance flexible TE cooling devices with $Bi_{0.5}Sb_{1.5}Te_3$/epoxy thick films through improving the (000 *l*) preferential orientation.

Acknowledgments

This work was supported by the National Natural Science Foundation of China (Nos. 51620105014, 51572210, 51521001 and 51502228) and National key Research And Development Plan of China (No. 2018YFB0703600). DSC, TG, XRD and FESEM experiments had performed at the Center for Materials Research and Testing of Wuhan University of Technology. The transport properties measurements had performed at State Key Lab of Advanced Technology for Materials Synthesis and Processing of Wuhan University of Technology.

References

[1] H.Y. Zhang, Y.C. Mui, M. Tarin, Analysis of thermoelectric cooler performance for high power electronic packages, Appl. Therm. Eng. 30 (2010) 561.
[2] R.E. Simons, M.J. Ellsworth, R.C. Chu, An assessment of module cooling enhancement with thermoelectric coolers, J. Heat Trans-T ASME 127 (2005), p. 76.
[3] M. Hines, J. Lenhardt, M. Lu, L. Jiang, Z.G. Xiao, Cooling effect of nanoscale Bi_2Te_3/Sb_2Te_3 multilayered thermoelectric thin films, J. Vac. Sci. Technol. A 30 (2012) 4.
[4] Z. Xiao, K. Hedgemen, M. Harris, E. DiMasi, Fabrication of Bi_2Te_3/Sb_2Te_3 and Bi_2Te_3/Bi_2Te_2Se multilayered thin film-based integrated cooling devices, J. Vac. Sci. Technol. A 28 (2010) 679.
[5] L.E. Bell, Cooling, heating, generating power, and recovering waste heat with thermoelectric systems, Science 321 (2008) 1457.
[6] J. Francis. DiSalvo, Thermoelectric cooling and power generation, Science 285 (1999) 703.
[7] I. Chowdhury, R. Prasher, K. Lofgreen, G. Chrysler, S. Narasimhan, R. Mahajan, D. Koester, R. Alley, R. Venkatasubramanian, On-chip cooling by superlattice-based thin-film thermoelectrics, Nat. Nanotechnol. 4 (2009) 235.
[8] F. Hao, P.F. Qiu, Y.S. Tang, S.Q. Bai, T. Xing, H.S. Chu, Q.H. Zhang, P. Lu, T.S. Zhang, D.D. Ren, J.K. Chen, X. Shi, L.D. Chen, High efficiency Bi_2Te_3-based materials and devices for thermoelectric power generation between 100 and 300 °C, Energy Environ. Sci. 9 (2016) 3120.
[9] Q.H. Zhang, X.Y. Huang, S.Q. Bai, X. Shi, C. Uher, L.D. Chen, Thermoelectric devices for power generation: recent progress and future challenges, Adv. Eng. Mater. 18 (2016) 194.
[10] Z.Y. Lu, M. Layani, X.X. Zhao, L.P. Tan, T. Sun, S.F. Fan, Q.Y. Yan, S. Magdassi, H.H. Hng, Fabrication of flexible thermoelectric thin film devices by inkjet printing, Small 10 (2014) 3551.
[11] D.L. Zhao, G. Tan, A review of thermoelectric cooling: materials, modeling and applications, Appl. Therm. Eng. 66 (2014) 15.
[12] W.Y. Zhao, Z.Y. Liu, P. Wei, Q.J. Zhang, W.T. Zhu, X.L. Su, X.F. Tang, J.H. Yang, Y. Liu, J. Shi, Y.M. Chao, S.Q. Lin, Y.Z. Pei, Magnetoelectric interaction and transport behaviors in magnetic nanocomposite thermoelectric materials, Nat. Nanotechnol. 12 (2017) 55.
[13] C.G. Fu, S.Q. Bai, Y.T. Liu, Y.S. Tang, L.D. Chen, X.B. Zhao, T.J. Zhu, Realizing high figure of merit in heavy-band p-type half-Heusler thermoelectric materials, Nat. Commun. 6 (2015) 7.
[14] L.D. Zhao, S.H. Lo, Y. Zhang, H. Sun, G. Tan, C. Uher, C. Wolverton, V.P. Dravid, M.G. Kanatzidis, Ultralow thermal conductivity and high thermoelectric figure of merit in SnSe crystals, Nature 508 (2014) 373.
[15] K. Biswas, J. He, I.D. Blum, C.I. Wu, T.P. Hogan, D.N. Seidman, V.P. Dravid, M.G. Kanatzidis, High-performance bulk thermoelectrics with all-scale hierarchical architectures, Nature 489 (2012) 414.
[16] H.L. Liu, X. Shi, F.F. Xu, L.L. Zhang, W.Q. Zhang, L.D. Chen, Q. Li, C. Uher, T. Day, G.J. Snyder, Copper ion liquid-like thermoelectrics, Nat. Mater. 11 (2012) 422.
[17] W.J. Xie, J. He, H.J. Kang, X.F. Tang, S. Zhu, M. Laver, S.Y. Wang, J.R.D. Copley, C.M. Brown, Q.J. Zhang, T.M. Tritt, Identifying the specific nanostructures responsible for the high thermoelectric performance of (Bi, $Sb)_2Te_3$ nanocomposites, Nano Lett. 10 (2010) 3283.
[18] H. Wu, X. Liu, P. Wei, H.Y. Zhou, X. Mu, D.Q. He, W.T. Zhu, X.L. Nie, W.Y. Zhao, Q.J. Zhang, Fabrication and characterization of brush-printed p-type $Bi_{0.5}Sb_{1.5}Te_3$ thick films for thermoelectric cooling devices, J. Electron. Mater. 46 (2017) 2950.
[19] D. Madan, A. Chen, P.K. Wright, J.W. Evans, Dispenser printed composite thermoelectric thick films for thermoelectric generator applications, J. Appl. Phys. 109 (2011) 034904.
[20] Z. Cao, E. Koukharenko, M.J. Tudor, R.N. Torah, S.P. Beeby, Flexible screen printed thermoelectric generator with enhanced processes and materials, Sens. Actuators A-Phys. 238 (2016) 196.
[21] Z. Cao, E. Koukharenko, R.N. Torah, J. Tudor, S.P. Beeby, Flexible screen printed thick film thermoelectric generator with reduced material resistivity, J. Phys. 557 (2014) 012016.
[22] D. Madan, Z.Q. Wang, A. Chen, R.C. Juang, J. Keist, P.K. Wright, J.W. Evans, Enhanced performance of dispenser printed MA n-type Bi_2Te_3 composite thermoelectric generators, ACS Appl. Mater. Interfaces 4 (2012) 6117.
[23] D. Madan, Z.Q. Wang, A. Chen, P.K. Wright, J.W. Evans, High-performance dispenser printed MA p-Type $Bi_{0.5}Sb_{1.5}Te_3$ flexible thermoelectric generators for powering wireless sensor networks, ACS Appl. Mater. Interfaces 5 (2013) 11872.
[24] S. Shin, R. Kumar, J.W. Roh, D.S. Ko, H.S. Kim, S.I. Kim, L. Yin, S.M. Schlossberg, S. Cui, J.M. You, S. Kwon, J.L. Zheng, J. Wang, R.K. Chen, High-performance screen-printed thermoelectric films on fabrics, Sci. Rep. 7 (2017) 9.
[25] L.H. Fan, B. Su, J.M. Qu, C.P. Wong, Electrical and thermal conductivities of polymer composites containing nano-sized particles, in: Proceedings of the 54th Electronic Components and Technology Conference, vol. 1, 2004, p.148.
[26] Y.F. Liu, Z.J. Du, C. Zhang, C.J. Li, H.Q. Li, Curing behavior and thermal properties of multifunctional epoxy resin with methylhexahydrophthalic anhydride, J. Appl. Polym. Sci. 103 (2007) 2041.
[27] F.K. Lotgering, Topotactical reactions with ferrimagnetic oxides having hexagonal crystal structures, J. Inorg. Nucl. Chem. 9 (1959) 113.
[28] X. Liu, W.Y. Zhao, H.Y. Zhou, X. Mu, D.Q. He, W.T. Zhu, P. Wei, H. Wu, Q.J. Zhang, Fabrication and optimization of brush-printed n-type Bi_2Te_3 thick films for thermoelectric cooling devices, J. Electron. Mater. 45 (2016) 1328.
[29] X. Mu, H.Y. Zhou, D.Q. He, W.Y. Zhao, P. Wei, W.T. Zhu, X.L. Nie, H.J. Liu, Q.J. Zhang, Enhanced electrical properties of stoichiometric $Bi_{0.5}Sb_{1.5}Te_3$ film with high-crystallinity via layer-by-layer in-situ Growth, Nano Energy 33 (2017) 55.
[30] C. Rajagopal, M. Stayam, Studies on electrical conductivity of insulator- conductor composites, J. Appl. Phys. 49 (1978) 5536.
[31] X. Guo, X.P. Jia, J.M. Qin, H.R. Sun, Y.W. Zhang, B. Sun, B.W. Liu, H.A. Ma, Fast preparation and high thermoelectric performance of the stable $Bi_{0.5}Sb_{1.5}Te_3$ bulk materials for different synthesis pressures, Chem. Phys. Lett. 610 (2014) 204.
[32] Y. Yu, D.S. He, S.Y. Zhang, O. Cojocaru-Miredin, T. Schwarz, A. Stoffers, X.Y. Wang, S.Q. Zheng, B. Zhu, C. Scheu, D. Wu, J.Q. He, M. Wuttig, Z.Y. Huang, F.Q. Zu, Simultaneous optimization of electrical and thermal transport properties of $Bi_{0.5}Sb_{1.5}Te_3$ thermoelectric alloy by twin boundary engineering, Nano Energy 37 (2017) 203.
[33] L.P. Hu, Y.M. Guo, J.Q. Li, W.Q. Ao, F.S. Liu, C.H. Zhang, Y. Li, X.R. Zeng, Control of donor-like effect in V_2VI_3 polycrystalline thermoelectric materials, Mater. Res. Bull. 99 (2017) 377.
[34] T.J. Zhu, L.P. Hu, X.B. Zhao, J. He, New insights into intrinsic point defects in V_2VI_3 thermoelectric materials, Adv. Sci. 3 (2016) 16.
[35] D. Suh, S. Lee, H. Mun, S.-H. Park, K.H. Lee, K.S. Wng, J.-Y. Choi, S. Baik, Enhanced thermoelectric performance of $Bi_{0.5}Sb_{1.5}Te_3$-expanded graphene composites by simultaneous modulation of electronic and thermal carrier transport, Nano Energy 13 (2015) 67.
[36] J.G. Simmons, Generalized formula for the electric tunnel effect between similar electrodes separated by a thin insulating film, J. Appl. Phys. 34 (1963) 1793.
[37] D. Madan, Z.Q. Wang, A. Chen, R. Winslow, P.K. Wright, J.W. Evans, Dispenser printed circular thermoelectric devices using Bi and $Bi_{0.5}Sb_{1.5}Te_3$, Appl. Phys. Lett. 104 (2014) 4.
[38] A. Chen, D. Madan, P.K. Wright, J.W. Evans, Dispenser-printed planar thick-film thermoelectric energy generators, J. Micromech. Microeng. 21 (2011) 8.
[39] H.Y. Zhou, X. Mu, W.Y. Zhao, D.G. Tang, P. Wei, W.T. Zhu, X.L. Nie, Q.J. Zhang, Low interface resistance and excellent anti-oxidation of Al/Cu/Ni multilayer thin-film electrodes for Bi_2Te_3-based modules, Nano Energy 40 (2017) 274.
[40] J.C. Chen, Z.J. Yan, L.Q. Wu, Nonequilibrium thermodynamic analysis of a thermoelectric device, Energy 22 (1997) 979.

[41] L.G. Chen, C. Wu, F.R. Sun, Heat transfer effect on the specific cooling load of refrigerators, Appl. Therm. Eng. 16 (1996) 989.
[42] Z.G. Xiao, X.S. Zhu, On-chip sensing of thermoelectric thin film's merit, Sensors 15 (2015) 17232.
[43] L.M. Goncalves, J.G. Rocha, C. Couto, P. Alpuim, G. Min, D.M. Rowe, J.H. Correia, Fabrication of flexible thermoelectric microcoolers using planar thin-film technologies, J. Micromech. Microeng. 17 (2007) 168.
[44] G.J. Snyder, J.R. Lim, C.K. Huang, J.P. Fleurial, Thermoelectric microdevice fabricated by a MEMS-like electrochemical process, Nat. Mater. 2 (2003) 528.
[45] L.W. da Silva, M. Kaviany, Fabrication and measured performance of a first-generation microthermoelectric cooler, J. Microelectromech. S. 14 (2005) 1110.
[46] Huang I-Yu, Lin Jr-Ching, She Kun-Dian, Li Ming-Chan, Chen Jiann-Heng, Kuo Jin-Shun, Development of low-cost micro-thermoelectric coolers utilizing MEMS technology, Sens. Actuators A-Phys. 148 (2008) 176.

Weikang Hou received his B.S. degree from Anhui University of Technology (AHUT) in 2015. He is pursuing his M.S. degree at State Key Laboratory of Advanced Technology for Materials Synthesis and Processing (SKATMSP) of Wuhan University of Technology (WUT), China. His main research interest is focused on the thermoelectric devices.

Xiaolei Nie received her M.S. degree from Tianjin University in 2012. Now she works as a laboratory technician at Center for Materials Research and Analysis of WUT, China. Her research focuses on the microanalysis and chemical composition analysis of thermoelectric materials.

Wenyu Zhao received his M.S. degree in 1996 at China University of Geosciences and Ph.D. in 2004 at WUT. He started to work at SKATMSP of WUT as a full professor since 2008. His research interests include thermoelectric materials, magnetic ferrite materials, magnetic thermoelectric materials, novel structure thermoelectric devices, and thermoelectric application technology.

Hongyu Zhou received his M.S. degree from Wuhan University of Technology (WUT) in 2012. He is pursuing his Ph.D. at State Key Laboratory of Advanced Technology for Materials Synthesis and Processing (SKATMSP) of WUT, China. His main research interests are the thermoelectric devices.

Xin Mu received his B.S. degree from WUT in 2012. Currently, he is pursuing his Ph.D. at SKATMSP of WUT, China. His research interest is focused on the low-dimensional thermoelectric materials.

Wanting Zhu received her M.S. degree from WUT in 2013. Now she works as a laboratory technician at Center for Materials Research and Analysis of WUT, China. Her research focuses on the morphology and structural characterization of thermoelectric materials.

Qingjie Zhang received his M.S. degree in 1984 and Ph.D. in 1990 from Huazhong University of Science and Technology. Currently, he is the president of WUT, director of SKATMSP, and chief scientist of National 973 Program in the field of thermoelectric materials. His research focuses on the thermoelectric materials and the related application technology.